PHYSICAL REVIEW A VOLUME 25, NUMBER 1 JANUARY 1982

Theory of intermittency

J. E. Hirsch
Institute for Theoretical Physics, University of California, Santa Barbara, California 93106

B. A. Huberman
Xerox Palo Alto Research Center, Palo Alto, California 94304

D. J. Scalapino
Department of Physics, University of California, Santa Barbara, California 93106

(Received 29 June 1981)

The aperiodic or chaotic behavior for one-dimensional maps just before a tangent bifurcation occurs appears as intermittency in which long laminarlike regions irregularly separated by bursts occur. Proceeding from the picture proposed by Pomeau and Manneville, numerical experiments and analytic calculations are carried out on various models exhibiting this behavior. The behavior in the presence of external noise is analyzed, and the case of a general power dependence of the curve near the tangent bifurcation is studied. Scaling relations for the average length of the laminar regions and deviations from scaling are determined. In addition, the probability distribution of path lengths, the stationary distribution of the maps, the correlation function and power spectrum of the map in the intermittent region, and the Lyapunov exponent are obtained.

I. INTRODUCTION

There has recently been considerable interest in the properties of nonlinear discrete maps.[1-3] Such maps arise in a variety of nonlinear field theories. Perhaps the best known of these is the Poincaré sections for dynamical systems which can be usefully approximated by such maps relating a continuous time process to a discrete process.[4] Spatial order for commensurate-incommensurate phase transitions on a lattice have recently been discussed in terms of discrete maps.[5,6] In addition, the phenomena of electron localization on a lattice with an incommensurate potential has been treated as a discrete mapping problem generated by the Hamiltonian acting on a tight-binding state.[7] In all these cases, there is a physical parameter which enters the map in an essential way. In a hydrodynamic system it could be the Reynolds or Prandtl number, for a phase transition it could be the ratio of near to next-near coupling constants, while in the quantum-mechanics problem it was the ratio of the hopping matrix element to the incommensurate potential. As this parameter is changed, the sequence of iterates generated from the map may alter going from a regular periodic to an irregular aperiodic or chaotic behavior at some critical value of the parameter. The nature of this transition to chaotic behavior forms the focus of much of the recent interest.[8] In particular, the concepts of scaling and universality[9] so successful in the theory of phase transitions play a central role, encouraging the detailed study of simple models.

Here we are interested in the onset of chaotic behavior characterized by the occurrence of regular or laminar phases separated by intermittent bursts. This intermittent transition to turbulence was discussed by Pomeau and Manneville[10] in connection with the Lorenz model. They pointed out that it arises when a tangent bifurcation occurs. A simpler model which exhibits this type of phenomena[11] is the well-known logistic map

$$x_{n+1}=R x_n(1-x_n) \tag{1.1}$$

with $0 \leq x \leq 1$ and $0 \leq R \leq 4$. The attractor for this map in the region $3 \leq R \leq 4$ is shown in Fig. 1. Past the first period doubling bifurcation cascade at $R=3.57$, various open regions with odd numbers of fixed points appear which arise from tangent bifurcations. The three-cycle region appears last at $R_c=1+\sqrt{8}$.[12] As R increases further one can see that this three-cycle behavior undergoes the usual cascade bifurcation to chaos. However,

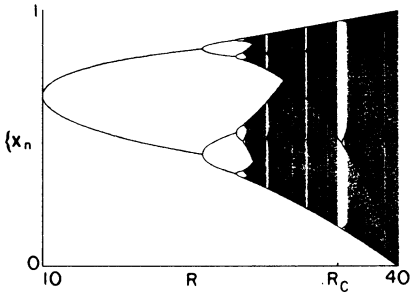

FIG. 1. The attractor vs R for the logistic map $x_{n+1}=Rx_n(1-x_n)$ (from Ref. 16). The intermittent behavior discussed in this paper arises when R decreases below the threshold for an odd-limit cycle. In particular, we focus on the region just below $R_c=1+\sqrt{8}$ which is the threshold for three-cycle orbits.

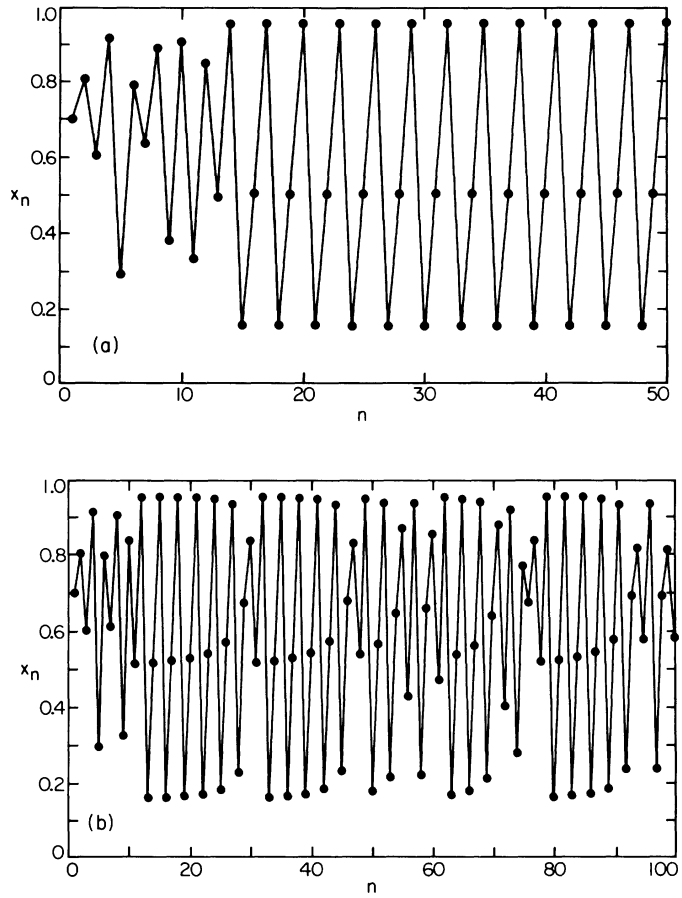

FIG. 2. Iterates of the logistic map starting from $x = 0.7$; (a) in the stable three-cycle region $R_c - R = -0.002$ and (b) in the intermittent region $R - R_c = 0.002$.

as R decreases below R_c the system also enters a chaotic regime and it is this transition, ocurring through intermittency, that we study here.

Figures 2(a) and 2(b) show the results of iterating Eq. (1.1) for $R = R_c + 0.002$ and $R = R_c - 0.002$, respectively. For $R > R_c$, after an initial transient, the iterates settle down to threefold limit cycle. However, for $R < R_c$, approximate threefold cycles are interrupted by irregular behavior. Figure 3 shows every third iterate for $R_c - R = 10^{-4}$ and nearly repeating segments of varying length l appear. These form the "laminar" regions separated by irregular behavior which appears as bursts if one magnifies the scale.

The geometric picture of Pomeau and Manneville which explains this phenomena can be illustrated by constructing the three-iterate map

$$F^{(3)}(x) = F(F(F(x))) \tag{1.2}$$

with $F(x) = Rx(1-x)$. This map is plotted in Fig. 4 for $R = R_c$. At this critical value the map is just tangent to the line x at $x = (0.160,\ 0.514,\ 0.956)$.

For $R > R_c$, $F^{(3)}(x)$ passes through the line x giving rise to six new fixed points of which three are stable. This is the phenomena of tangent bifurcation and the manner in which odd-limit cycles enter the attractor. Figure 5 shows a blowup of the region near $x_c = 0.514$ for $R = R_c - 5 \times 10^{-3}$. The

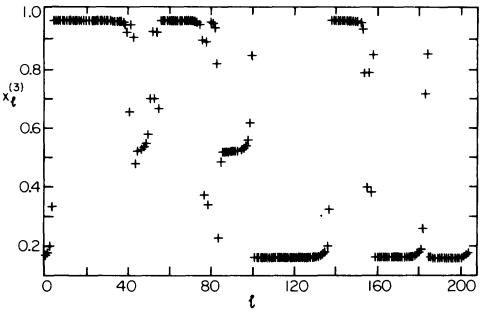

FIG. 3. Third iterate of the logistic map for $R_c - R = 0.0001$ showing regions of laminar behavior by intermittent irregularities.

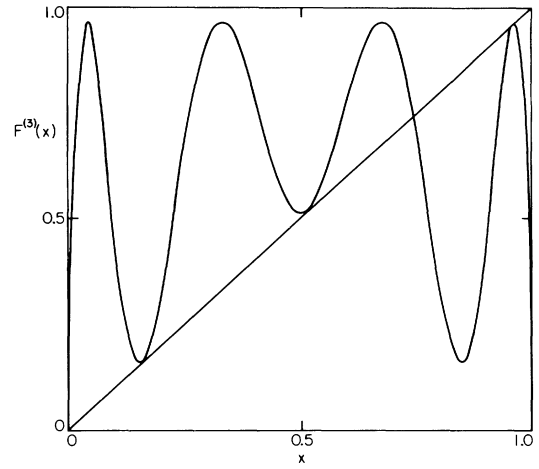

FIG. 4. The threefold iterated map $F^{(3)}(x)$ vs x for $R = R_c$.

points represent a sequence of threefold iterates which map in the usual way indicated by the staircase path. The slow passage of the iterates as x approaches $x_c = 0.514$ is evident. Pomeau and Manneville pointed out that as $R \to R_c$, this time of passage diverges as $(R_c - R)^{-1/2}$. After passing through the region shown in Fig. 5, the iterates move wildly under the map until they return to this neighborhood or a similar one near 1.160 and 0.956. This produces the regular laminarlike regions separated by bursts shown in Figs. 2(b) and 3 which are characteristic of the intermittent region.

In order to test this idea against experiment it is useful to consider what can be measured. Clearly, given a gate G which sets an acceptance $|x - x_c| < G$ on deviations in the laminar region, the average number of threefold iterates or length $\langle l \rangle$ can be determined. In addition, one

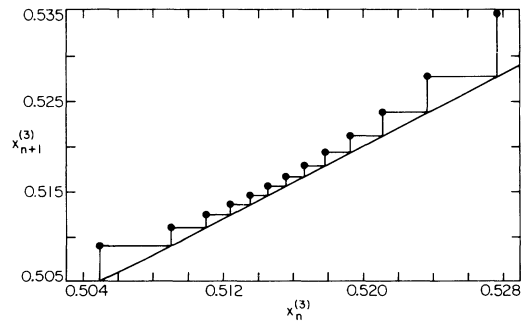

FIG. 5. A blowup of the central region of Fig. 4 showing $F^{(3)}(x)$ for $R_c - R = 0.005$. Successive third iterates of a point show the phenomena of slow passage which gives rise to the laminarlike regions in Figs. 2(b) and 3.

could imagine determining $P(l)$, the probability of a laminar region of length l. Beyond this it would be natural to observe the correlation function

$$C(l) = \frac{1}{N} \sum_{n=1}^{N} \langle x_{n+l}\, x_n \rangle \tag{1.3}$$

and/or its power spectrum

$$S(\omega_k) = C(0) + 2 \sum_{l=1}^{N-1} C(l) \cos(l\omega_k) + C(N) \cos N\omega_k , \tag{1.4}$$

where $\omega_k = 2\pi k/N$. Finally, if the system appeared to be in a steady state, one might try to find the probability $W(x)$ of finding the system with a given value x.

In addition to these observables, one might even devise an experimental observation of the Lyapunov exponent λ. This is usually introduced as a formal parameter useful in characterizing the sensitivity to initial conditions:

$$\lim_{N\to\infty} e^{N\lambda} = \lim_{N\to\infty} \lim_{\Delta\to 0} \{[x_N(x_0 + \Delta) - x_N(x_0)]/\Delta\} . \tag{1.5}$$

Here x_N is the Nth iterate and $x_0 + \Delta$ and x_0 are two neighboring points. Clearly, if λ is positive, two nearby points separate at an exponential rate, if λ is negative, they converge towards a fixed point. Although here we are primarily interested in readily accessible experimental quantities, one must not be too hasty to judge what can and what cannot be observed. If, for example, light absorption produced two neighboring triplet states which could subsequently recombine depending upon their distance of separation, one might by a careful examination of the tail of the intensity-intensity correlation of their recombination radiation determine λ.

When observations are compared with theory it is also essential to understand the role of noise. This is particularly true in the case of chaotic phenomena which by their nature may appear noisy. There has in fact been considerable progress recently on understanding the effects of stochastic noise on maps near the bifurcation cascade to chaos.[13-16] For example, the Lyapunov exponent has been shown to satisfy a scaling behavior characterized by universal exponents. Here we will study the stochastic difference equation

$$x_{n+1} = R x_n (1 - x_n) + g\xi_n \tag{1.6}$$

with ξ_n a Gaussian random variable with $\langle \xi_n \rangle = 0$ and $\langle \xi_n \xi_n' \rangle = \delta'_{nn}$. In the presence of noise we find that as $\epsilon = (R_c - R) \to 0$, the ratio of the average length in the presence of noise to that with $g = 0$ scales as[17]

$$\frac{\langle l \rangle_\alpha}{\langle l \rangle_0} = f(\alpha) \tag{1.7}$$

with α proportional to $g^2/\epsilon^{3/2}$ for Eq. (1.6) or more generally for $F^{(3)}(x)$ maps which have a quadratic term when expanded about their point of contact x_c (see Fig. 4). If this term vanishes and the lowest-order term beyond the linear $(x-x_c)$ term is $(x-x_c)^z$, then we find that

$$\langle l\rangle_0 \sim \epsilon^{-(z-1)/z} \quad \text{and} \quad \alpha \sim g^2/\epsilon^{(z+1)/z}.$$

The layout of the paper proceeds as follows. In Sec. II, the results of a variety of numerical experiments on the logistic map are presented. With these results in mind, a simple theoretical model is proposed and analyzed in Sec. III. Results for $\langle l\rangle$, $P(l)$, and $W(x)$ are obtained. In addition, the effect of noise on these results is investigated. Exact results as well as the $\epsilon \to 0$ scaling limits are derived. In addition, these theoretical results are compared with results of numerical experiments on a simple map constructed to exhibit the important features of the intermittent transition to chaos. A brief conclusion is given in Sec. IV.

II. NUMERICAL RESULTS FOR THE LOGISTIC MAP

In order to explore the phenomena of intermittency, we carried out a number of numerical experiments using the logistic map. In Fig. 6, observations of the average number $\langle l\rangle$ of threefold iterations which begin and end inside an acceptance gate $G = |x-x_c| = 10^{-2}$ are plotted versus ϵ. These data were obtained from runs in which 10^4 laminar regions were observed. A laminar region

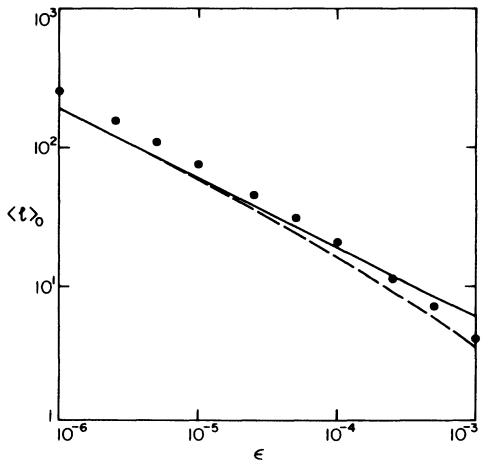

FIG. 6. The dots show the average number $\langle l\rangle$ of threefold iterations measured between bursts for the logistic map vs ϵ for an acceptance gate $|x-x_c| < 10^{-2}$. The dashed line corresponds to Eq. (3.9) and the solid line is its asymptotic limit $\epsilon/|x-x_c| \to 0$ given by Eq. (3.10).

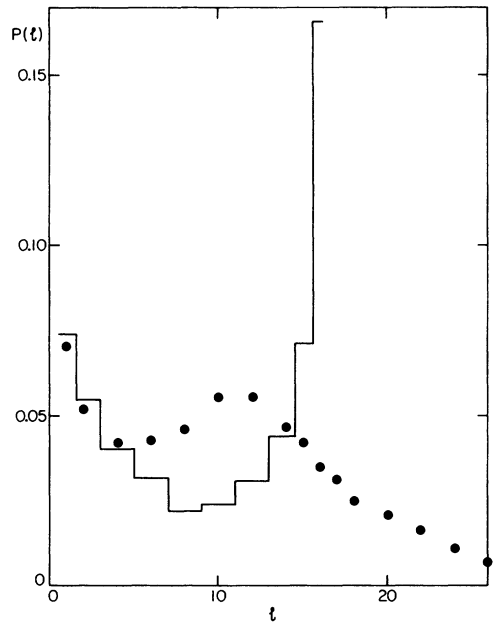

FIG. 7. The histogram shows the measured probability distribution $P(l)$ for having laminar regions $3l$ iterates long for $\epsilon = 2.5\times10^{-4}$ in the absence of stochastic noise, $g = 0$. The dots show $P(l)$ for the same value of ϵ but with $g = 5\times10^{-4}$. In both cases the acceptance gate was $|x-x_c| < 10^{-2}$.

of length l occurs if an iterate falls inside the gate $|x_n - x_c| < G$ and leaves after l threefold iterates. Deviations of runs starting from different initial values of x were of order 1%. For $\epsilon < 10^{-4}$, the measured values of $\langle l\rangle$ clearly follow the expected $\epsilon^{-1/2}$ behavior. The solid and dashed lines are the results of analytic calculations for a model discussed in Sec. III.

For $\epsilon = 2.5\times10^{-4}$, the probability distribution $P(l)$ for lengths of a given run was computed and is plotted as the histogram versus l in Fig. 7. The

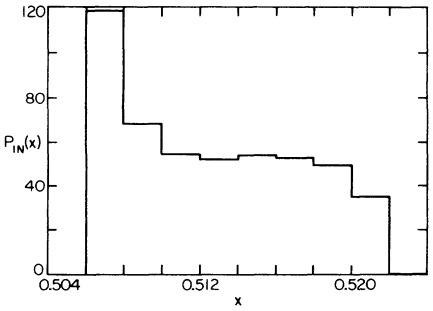

FIG. 8. The probability $P_{in}(x)$ of a given starting value of x inside the acceptance gate for $\epsilon = 2.5\times10^{-4}$. Note that this peaks at the lower end of the gate skewing $P(l)$ shown in Fig. 7 towards larger l values.

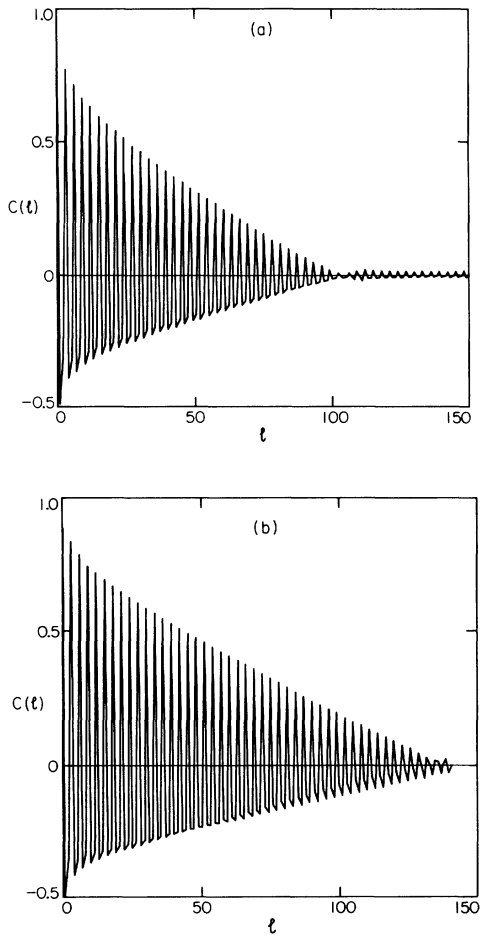

FIG. 9. The correlation function $C(l) = \langle x_{n+L} x_n \rangle$ averaged over 10^6 iterates of the logistic map. (a) $\epsilon = 10^{-4}$, (b) $\epsilon = 5 \times 10^{-5}$. Straight lines are drawn between the points.

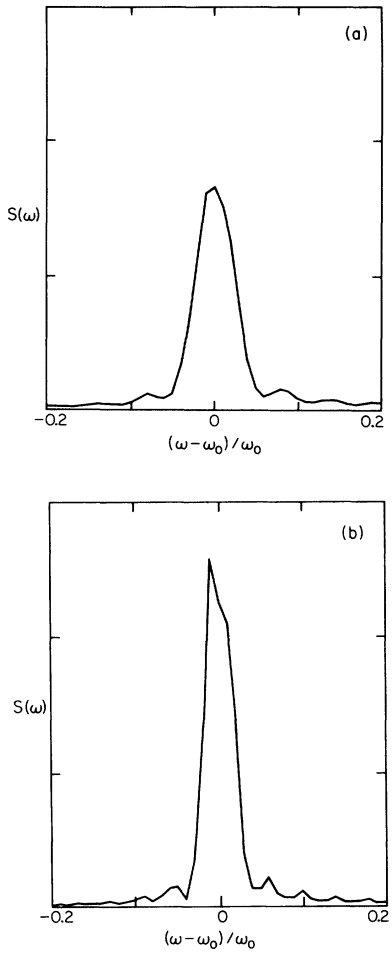

FIG. 10. The power spectra of the correlation functions of Fig. 9, $\omega_0 = 2\pi/3$.

shape of this distribution simply reflects the fact that there is only a narrow region $\sim\epsilon^{1/2}$ about x_c for which the path length will be close to the average. Most of the starting points are on one side or the other of the bottleneck. If the feed into the region within the acceptance gate $|x - x_c| \leq G$ were white, we would expect that $P(l)$ would be symmetric about $l = \langle l \rangle$. However, the minimum in $F^{(3)}(x)$ just below x_c (see Fig. 4) causes the input distribution $P_{in}(x)$ to be peaked towards the lower end of the acceptance region $x = x_c - G$ and skews $P(l)$ towards large l values. This distribution $P_{in}(x)$ is shown as the histogram in Fig. 8 for $\epsilon = 2.5 \times 10^{-4}$.

Correlation functions $C(l)$, Eq. (1.3), obtained from averaging $\langle x_{n+l} x_n \rangle$ over 10^6 iterates for two values of ϵ are shown in Fig. 9. These were normalized so that $C(0) = 1$. Clearly as ϵ decreases the correlation length characteristic of the decay increases. It follows an $\epsilon^{-1/2}$ behavior as one would expect. The power spectrum $S(\omega)$ obtained by Fourier transforming these correlation functions are shown in Fig. 10. In the transition to chaos via intermittency, the power spectrum changes continuously from a delta function to a broadened peak whose width varies approximately as $\epsilon^{1/2}$ as R decreases below R_c. This is quite different from the behavior which occurs just above the bifurcation cascade into the chaotic regime where sharp delta-funtion-like spikes remain with broadband noise rising up as a background.[16]

In order to study the effect of noise on the intermittency transition to chaotic behavior, a stochastic term was added to the logistic map, Eq. (1.6). By selecting g, the effect of different noise levels could be studied. Here ξ_n was a pseudo random variable selected in the region $(-\frac{1}{2}, \frac{1}{2})$ so that the variance of the noise term was $g^2/12$. According to the theory discussed in Sec. III, the appropriate scaling variable is $g^2/\epsilon^{3/2}$. In

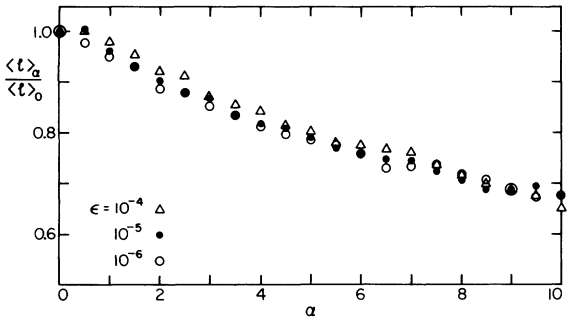

FIG. 11. The average length of the three-iterate laminar regions $\langle l\rangle_{\alpha'}$ for the logistic map in the presence of noise $\alpha' = 10g^2/\epsilon^{3/2}$ normalized to its zero noise value $\langle l\rangle_0$ for three different values of ϵ. Note the approximate scaling of the data when it is plotted in this way.

Fig. 11 the results for the ratio of the average length $\langle l\rangle'_\alpha$ in the presence of noise $\alpha' = 10g^2/\epsilon^{3/2}$ to its value $\langle l\rangle_0$ in the absence of noise is plotted as a function of α' for different values of ϵ. Once again 10^4 laminar regions were obtained in a given run leading to rms errors of order 1%. It is clear that the results for $\epsilon = 10^{-4}$ to $\epsilon = 10^{-6}$ are very similar to each other when plotted in this way. There are in fact expected to be small differences proportional to ϵ but we will postpone discussions of deviations from scaling until Sec. III. Just as in the theory of phase transitions, the existence of scaling results in a great economy in dealing with data and, moreover, provides the framework for extracting the intrinsic chaotic behavior from the fluctuations produced by external noise.

The effect of noise on the distribution $P(l)$ of laminar lengths is shown as the dots in Fig. 7. The tail giving values of l exceeding $l_{\max}$ for $g=0$ results from a passage in which the noise shifts the point back of the bottleneck region after it has already passed through it.

Writing $x_N(x_0) = F^{(N)}(x_0)$ and using the chain rule for differentiation one has for the Lyapunov exponent, Eq. (1.5),

$$\lambda = \lim_{N\to\infty} \frac{1}{N} \sum_{i=1}^{N} \ln[R(1-2x_i)] . \tag{2.1}$$

For $\epsilon < 0$, the system settles down to the three-cycle behavior shown in Fig. 2(a) and

$$\lambda = \tfrac{1}{3} \sum_{i=1}^{3} \ln[R(1-2x_i)] . \tag{2.2}$$

Here x_1, x_2, and x_3 are the stable three-cycle fixed points for a given $R > R_c$. Results obtained for λ versus ϵ for the logistic map are shown in Fig. 12. The solid line shows λ in the absence of any stochastic noise, $g=0$. Figure 13 shows $\ln|\lambda|$ versus $\ln|\epsilon|$ for $g=0$. Here the solid dots correspond to the divergent, intermittent region with $\epsilon > 0$ ($R < R_c$) where $\lambda > 0$ and the open circles correspond to the stable three-cycle region with $\epsilon < 0 (R > R_c)$ where $\lambda < 0$. For $\epsilon < 0$ it is straightforward to show that

$$\lambda = -\tfrac{2}{3}(a_c b_c)^{1/2} |\epsilon|^{1/2} + O(|\epsilon|) , \tag{2.3}$$

where a_c and b_c are given by Eq. (3.2). This is shown as the dashed line in Fig. 13. When $\epsilon > 0$, we know that the number of steps in the bottleneck region varies as $\epsilon^{-1/2}$ so that we expect that $\lambda \sim \epsilon^{1/2} + O(\epsilon)$. The solid line in Fig. 13 varies as $\epsilon^{1/2}$ and

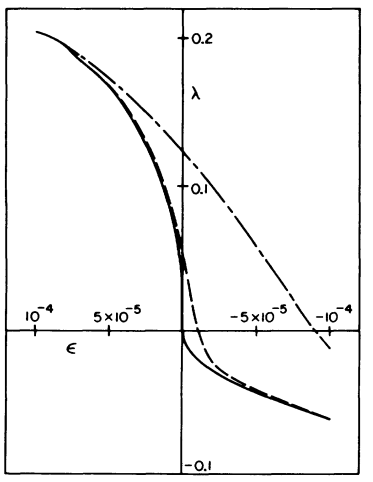

FIG. 12. The Lyapunov exponent λ vs ϵ for the logistic map. The solid curve is without noise $g=0$ while the dashed and dash-dot curve are with noise $g = 10^{-4}$ and 5×10^{-4}, respectively.

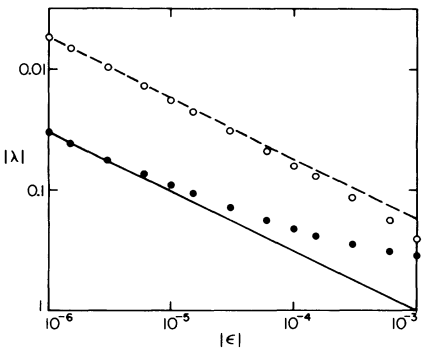

FIG. 13. A log-log plot of $|\lambda|$ vs $|\epsilon|$ for the logistic map in the absence of noise. The solid dots are for $\epsilon > 0$ and correspond to divergent trajectories with $\lambda > 0$ while the open circles are for $\epsilon < 0$ and correspond to stable three-cycle trajectories with $\lambda < 0$.

has been adjusted to fit the data for small ϵ. Note that the "critical" region in which $\epsilon \sim \epsilon^{1/2}$ for $\epsilon > 0$ is very narrow due to the contribution from the burst regions. Compare this with the behavior of $\langle l \rangle_0$ shown in Fig. 6 which has the asymptotic form $\epsilon^{1/2}$ for $\epsilon \lesssim 10^{-4}$. The effect of noise is to wash out the $\epsilon = 0$ singularity as shown in Fig. 12. In the critical region we find that λ scales with $g^2/\epsilon^{3/2}$ just as $\langle l \rangle_\alpha$ does.

Having explored some of the basic phenomena exhibited by a particular map near the intermittency threshold, we turn in the next section to an analysis of a simple model which contains the essential features of the geometrical picture introduced by Pomeau and Manneville.

III. ANALYTIC FORMULATION AND RESULTS

In this section we discuss a simple analytic formulation of the intermittency problem in the presence of external noise; we consider the recursion relation

$$y' = y + ay^z + \epsilon + g\xi \,. \tag{3.1}$$

Such a recursion relation arises in the logistic map when expanding around the contact point. Near the region of the tangent bifurcation, $F^{(3)}(x, R)$ can be expanded about x_c and R_c,

$$F^{(3)}(x,R) \cong x_c + (x - x_c) + a_c(x - x_c)^2 + b_c(R_c - R) \,. \tag{3.2}$$

Here x_c is one of the three contact points where $R = R_c$. Although the parameters a_c and b_c are in fact different from the middle contact point and the two outer contact points, their product $a = a_c b_c = 68.5$ which enters in various physical predictions is identical for all three regions. Setting $y = (x - x_c)/b_c$ and including an external noise gives a recursion relation for the threefold iterate having the form of Eq. (3.1) with $z = 2$. If the coefficient a_c of the quadratic term in Eq. (3.2) were to vanish one would need to include the first nonvanishing term $(x - x_c)^z$. We will discuss mainly the case $z = 2$ here for definiteness, although the extension to arbitrary (positive and even) z is straightforward. The exponent z is important since it determines the "universality class" of the problem.

We will assume Eq. (3.1) to be valid only over a small range of the variable y, $-y_0 < y < y_0$. Outside this range, we assume the variable y to undergo some unknown chaotic motion for some time and then to reenter again the interval of interest. In general, this reentry will occur at random points y_{in} subject to some probability distribution which depends on the model under consideration; a particular example was discussed in Sec. II. For purposes of the theory the detailed form of $P_{in}(y)$ is irrelevant and we will assume the simplest possible form, i.e., "white" reentry:

$$P_{in}(y) = \frac{1}{2y_0} - y_0 < y < y_0 \,. \tag{3.3}$$

The external noise ξ is assumed to be a random variable with

$$\langle \xi \rangle = 0 \,, \tag{3.4a}$$

$$\langle \xi^2 \rangle = 1 \,. \tag{3.4b}$$

The quantities of interest in the problem do not depend on the form of the distribution of ξ, so that we will take it to be uniformly distributed for our numerical experiments.

In order to treat the problem analytically, we approximate the recursion relation (3.1) by a differential equation on which the step spacing is dt,

$$\frac{dy}{dt} = ay^z + \epsilon + g\xi(t) \,. \tag{3.5}$$

Here $\xi(t)$ is a Gaussian white noise source, satisfying

$$\langle \xi(t)\xi(t') \rangle = \delta(t - t') \,. \tag{3.6}$$

The passage from (3.1) to (3.5) is justified if the changes in y at each step are small. This will always be the case for small ϵ and y_0. Since we are interested in the limit of small ϵ, and the value of y_0 is at our disposal, this approximation is not essential for our results. This is confirmed by the results of our numerical experiments using Eq. (3.1), which closely agree with the analytic result obtained from (3.5).

We now discuss some of the results one can derive from these recursion relations, first in the absence of external noise.

A. Intermittency in the absence of external noise

Consider first the case $z = 2$. The differential equation is

$$\frac{dy}{dt} = ay^2 + \epsilon \,. \tag{3.7}$$

This is readily integrated to yield

$$l(y_{in}) = \frac{1}{\sqrt{a\epsilon}} \left[\arctan\left(\frac{y_0}{\sqrt{\epsilon/a}}\right) - \arctan\left(\frac{y_{in}}{\sqrt{\epsilon/a}}\right) \right] \tag{3.8}$$

for the length of time (number of steps) it takes a process started at y_{in} to reach the boundary y_0. Note that for $y_{in} < 0$ this diverges as $1/\sqrt{\epsilon}$ in the small-ϵ limit, as discussed by Pomeau and Manneville. The average time of passage is obtained by averaging (3.8) over the probability distribution of y_{in}. For the particular example of $P_{in}(y)$ chosen one gets

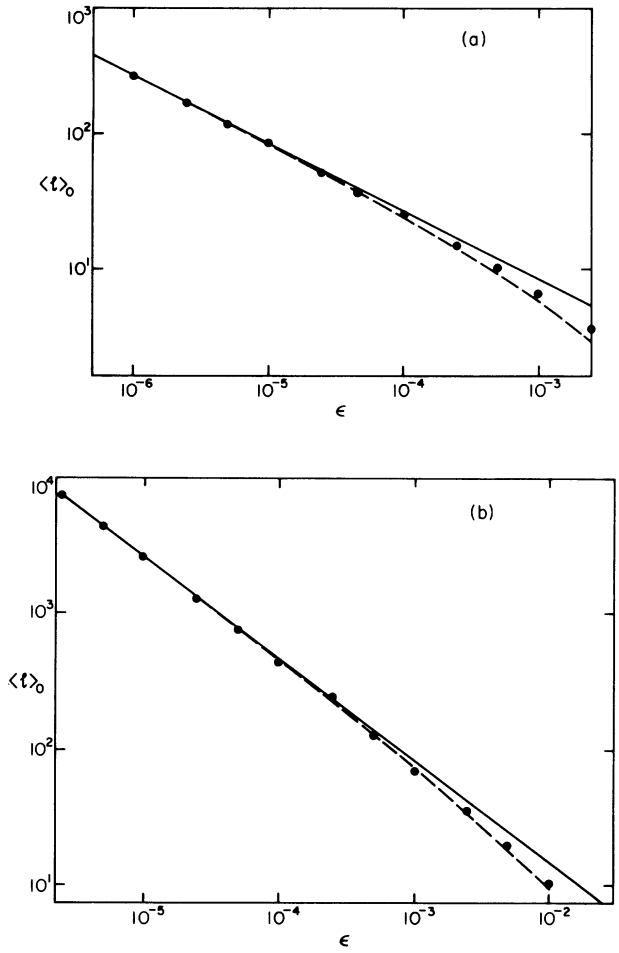

FIG. 14. Average time of passage $\langle l \rangle$ vs ϵ in the absence of external noise for (a) $z = 2$ and (b) $z = 4$. The dashed lines are the theoretical results from Eq. (3.11), the full lines are limiting forms for $\epsilon/y_0 \to 0$. The dots are results of numerical experiments with 10 000 passes per point. In this and the following figures, the numerical simulations were done using the map (3.1) with $a = 34$ and white reinjection, with a gate $y_0 = 0.01$ for $z = 2$ and $g_0 = 0.1$ for $z = 4$.

$$\langle l \rangle = \frac{1}{\sqrt{a\epsilon}} \arctan\left(\frac{y_0}{\sqrt{\epsilon/a}}\right) \tag{3.9}$$

and, in the limit of $\sqrt{\epsilon/a} \ll y_0$,

$$\langle l \rangle = \frac{\pi}{2} \frac{1}{\sqrt{a\epsilon}} . \tag{3.10}$$

For the case of general z, an identical calculation yields

$$\langle l \rangle = \frac{1}{2} \frac{1}{a^{1/z}} \frac{1}{\epsilon^{1-1/z}} \int_{-y_0/(\epsilon/a)^{1/z}}^{y_0/(\epsilon/a)^{1/z}} \frac{dx}{x^z+1} \tag{3.11}$$

so that the asymptotic behavior for small ϵ is

$$\langle l \rangle \propto 1/\epsilon^{(1-1/z)} \tag{3.12}$$

and in particular, for $z = 4$

$$\langle l \rangle = \frac{\pi}{\sqrt{8}} \frac{1}{a^{1/4}} \frac{1}{\epsilon^{3/4}} . \tag{3.13}$$

In Figs. 14(a) and 14(b) we plot the average time of passage for $z = 2$ and $z = 4$, respectively, in a log-log plot. The full lines are the "scaling limit" results (3.10) and (3.13) while the dashed lines are the "exact" results (3.11). The dots were obtained from numerical experiment on the discrete recursion relation Eq. (3.1) with the "boundary condition" that each time y goes out of the interval, it is reinjected randomly and uniformly between $-y_0$ and y_0. The results were averaged over 10 000 passes. It can be seen that the agreement between theory and "experiment" is excellent. Similarly, in Fig. 6, the solid line is the asymptotic form Eq. (3.10) and the dashed line corresponds to Eq. (3.9). In the case of the full logistic map, while the numerical data for $\langle l \rangle$ vary as $\epsilon^{-1/2}$, they have been shifted to larger values because the input into the acceptance region is not white (see Fig. 8). In the present section,

all numerical experiments were performed using Eq. (3.1) with a white reentering distribution.

It is also of interest to compute the probability distribution of path lengths, $P(l)$, where $P(l)dl$ gives the probability to observe a path with length between l and $l+dl$. Using the relation

$$P(l)dl = P_{\text{in}}(y_{\text{in}})dy_{\text{in}} \tag{3.14}$$

together with (3.8) and (3.3), one finds readily

$$P(l) = \frac{\epsilon}{2y_0}\left\{1+\tan^2\left[\arctan\left(\frac{y_0}{\sqrt{\epsilon/a}}\right) - \sqrt{\epsilon a}\, l\right]\right\}. \tag{3.15}$$

This is plotted in Fig. 15 for a particular case, $\epsilon = 10^{-5}$, as a dashed line: the histogram is the result of a numerical experiment. It is interesting to note that in the absence of noise the average value of l is actually the least likely to occur. The most likely paths are either very short or close to the maximum value given by

$$l_{\max} = \frac{2}{\sqrt{\epsilon a}}\arctan\left(\frac{y_0}{\sqrt{\epsilon/a}}\right). \tag{3.16}$$

The observation may be important from an experimental point of view. Similar results are obtained for the general z case. However, we should note that this behavior changes in the presence of external noise; this will be discussed further in the following subsection.

B. Intermittency in the presence of external noise

Consider now the differential equation (3.5) with the external noise present. As is well known, for a Langevin process of the type described by (3.5) one can write the corresponding Fokker-Planck equation[18] for the time evolution of the probability distribution $W(y,t)$ for y:

$$\frac{d}{dt}W(y,t) = -\frac{d}{dy}[K_1(y)W(y,t)] + \frac{1}{2}\frac{d^2}{dy^2}[K_2(y)W(y,t)]. \tag{3.17}$$

Here we have for the moment neglected the reentering flux. The functions $K_1(y)$ and $K_2(y)$ are defined by

$$K_i(y) = \lim_{\tau\to 0}\frac{\langle[y(t+\tau)-y(t)]^i\rangle}{\tau}. \tag{3.18}$$

From (3.5) and (3.6) we obtain (for the case $z=2$)

$$K_1(y) = ay^2+\epsilon, \tag{3.19a}$$

$$K_2(y) = g^2. \tag{3.19b}$$

Equation (3.17) can be simply interpreted as a continuity equation

$$\frac{d}{dt}W(y,t) = -\frac{dG(y)}{dy} \tag{3.20}$$

that expresses the conservation of probability, where

$$G(y) = K_1(y)W(y,t) - \frac{1}{2}\frac{d}{dy}[K_2(y)W(y,t)] \tag{3.21}$$

is the probability current.

In order to take the reentering flux into account, Eq. (3.20) has to be modified to

$$\frac{d}{dt}W(y,t) = -\frac{dG(y)}{dy} + r. \tag{3.22}$$

Here, r is the rate at which the points reenter the interval per unit length, which is independent of y in our model. Equation (3.22) simply expresses the fact that $W(y,a)$ changes both due to the flow from neighboring points and the flow from outside.

First let us consider stationary solutions to (3.22). We have for our problem

$$(ay^2+\epsilon)W(y) - \tfrac{1}{2}g^2\frac{dW(y)}{dy} = G_0 + ry, \tag{3.23}$$

where G_0 is an integration constant arising from integrating (3.22) once. The appropriate boundary conditions are

$$W(-y_0) = W(y_0) = 0 \tag{3.24}$$

plus a normalization condition to determine r. Note that the current as a function of y is

$$G(y) = G_0 + ry. \tag{3.25}$$

The net number of points that leave the interval $(-y_0, y_0)$ per unit time is

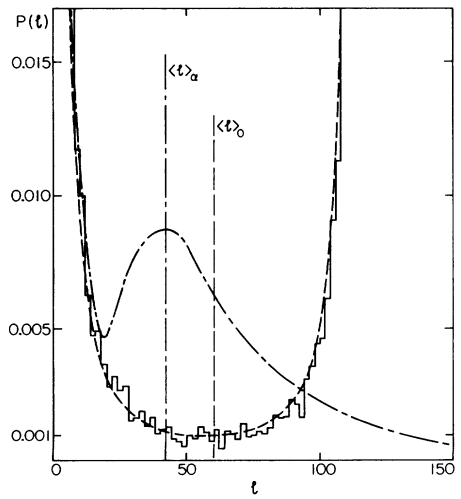

FIG. 15. Probability distributions of path lengths $P(l)$ vs l for $z=2$, $\epsilon = 10^{-5}$. Dashed line: theoretical results without noise. Histogram: results of a numerical simulation without noise. Dash-dotted line: numerical simulation in the presence of noise $\alpha = 100$.

$$N = G(y_0) - G(-y_0) = 2ry_0 \tag{3.26}$$

which equals the reentering density rate (r) times the length of the interval ($2y_0$). This expresses the conservation of probability in the more general sense discussed here.

It is convenient to rescale (3.23) as follows. Define

$$\begin{aligned} x &= y/\sqrt{\epsilon}\ , \\ W(x) &= \sqrt{\epsilon}\, W(y(x))\ , \\ \alpha &= g^2/\epsilon^{3/2}\ , \\ g_0 &= G_0/\sqrt{\epsilon}\ . \end{aligned} \tag{3.27}$$

Equation (3.23) then becomes

$$(1+ax^2)W(x) - \tfrac{1}{2}\alpha \frac{dW}{dx} = g_0 + rx\ , \tag{3.28}$$

which is readily integrated to yield

$$W(x) = \frac{2}{\alpha} r \int_x^{x_2} dx'(x - x_1 + c) \times \exp\{-(2/\alpha)[x' - x + (a/3)(x'^3 - x^3)]\}$$

with

$$x_2 = -x_1 = y_0/\sqrt{\epsilon}\ . \tag{3.30}$$

Here, c is determined by the boundary condition

$$W(x_1) = 0 \tag{3.31}$$

while r is determined by the normalization condition

$$\int_{x_1}^{x_2} dx\, W(x) = 1\ . \tag{3.32}$$

In Fig. 16 the stationary probability distribution is plotted for a particular case ($\epsilon = 10^{-5}$), with and without noise. The agreement between the results of the integral (3.29) and results of numerical experiments is very good. In the absence of noise, the probability distribution is simply

$$W(y) = \frac{\sqrt{\epsilon a}}{\pi y_0} \frac{y + y_0}{ay^2 + \epsilon} \tag{3.33}$$

and the most probable value of y is

$$y_m = \frac{\epsilon}{2y_0 a}\ . \tag{3.34}$$

Note that in the presence of noise the most probable value shifts appreciably to negative values of y.

Next, we consider the evaluation of the average length of passage in the presence of noise.[19] Consider a process $y(t)$ starting at a given y_{in} at time $t = 0$; the probability density for the process satisfies

$$W(y, t=0) = \delta(y - y_{in})\ . \tag{3.35}$$

We consider now in $W(y, t)$ only processes that have not reached the boundary in the time interval $(0, t)$. This probability density will satisfy the Fokker-Plank equation (3.17) in the interval $(-y_0, y_0)$. The integral

$$W(t) = \int_{-y_0}^{y_0} dy\, W(y, t) \tag{3.36}$$

gives the total probability that the process $y(t)$ did not reach the boundary until time t. Clearly, $W(t)$ satisfies

$$\begin{aligned} &W(0) = 1\ , \\ &W(t) \underset{t\to\infty}{\longrightarrow} 0\ . \end{aligned} \tag{3.37}$$

The dependence of $W(t)$ on y_{in} is understood. The probability of having a time of passage between t and $t + dt$ is clearly

$$w(t)dt = W(t) - W(t + dt) = -\frac{dW}{dt}dt \tag{3.38}$$

so that the mean first-passage time for a process that started at y_{in} at $t = 0$ is

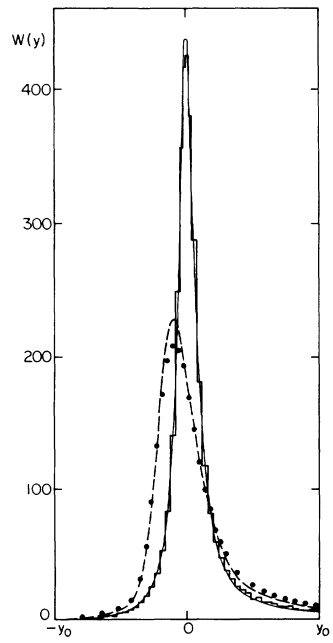

FIG. 16. Stationary probability distribution $W(y)$ for $z = 2$, $\epsilon = 10^{-5}$. The full and dashed lines are the theoretical results for $\alpha = 0$ and $\alpha = 100$, respectively. The histogram and the dots are the corresponding results from numerical experiments.

$$M(y_{in}) = \int_0^\infty dt\, w(t) t$$
$$= -\int_0^\infty dt \frac{dW}{dt} t$$
$$= \int_0^\infty dt\, W(t) . \tag{3.39}$$

Finally, we will be interested in the averaged first-passage time, obtained by averaging over y_{in}:

$$\langle l \rangle = \frac{1}{2y_0} \int_{-y_0}^{y_0} dy\, M(y) . \tag{3.40}$$

To find an equation satisfied by $M(y)$ it is useful to consider the adjoint equation to (3.17), the Kolmogoroff equation,[19] given by

$$\frac{d}{dt} W(y,t) = K_1(y_{in}) \frac{dW(y,t)}{dy_{in}} + \tfrac{1}{2} K_2(y_{in}) \frac{d^2 W(y,t)}{dy_{in}^2} , \tag{3.41}$$

where $W(y,0)$ satisfies the initial condition (3.35). Integrating (3.41) with respect to y we obtain, using (3.36),

$$\frac{d}{dt} W(t) = K_1(y_{in}) \frac{dW(t)}{dy_{in}} + \tfrac{1}{2} K_2(y_{in}) \frac{d^2 W(t)}{dy_{in}^2} \tag{3.42}$$

and integrating (3.42) in time from $t=0$ to $t=\infty$ and using (3.39) and (3.37) we find

$$-1 = (ay^2 + \epsilon) \frac{dM}{dy} + \tfrac{1}{2} g^2 \frac{d^2 M}{dy^2} , \tag{3.43}$$

where we have also specialized to the problem of interest here. We see that the problem reduces again to solving an ordinary differential equation.

Using the rescaling given by Eq. (3.27), with $m(x) = \sqrt{\epsilon} M(y(x))$, Eq. (3.43) takes the form

$$(ax^2 + \epsilon) \frac{dm}{dx} + \tfrac{1}{2} \alpha \frac{d^2 m}{dx^2} = -1 . \tag{3.44}$$

The appropriate boundary conditions are

$$m(x_1) = m(x_2) = 0 ,$$
$$x_2 = -x_1 = y_0/\sqrt{\epsilon} , \tag{3.45}$$

and the average time of passage is

$$\langle l \rangle_\alpha = \frac{1}{2y_0} \int_{-y_0/\sqrt{\epsilon}}^{y_0/\sqrt{\epsilon}} dx\, m(x, \alpha) . \tag{3.46}$$

For $\alpha = 0$ one has, as discussed in Sec. III A,

$$m(x, \alpha = 0) = \frac{1}{\sqrt{a}} (\arctan x_2 - \arctan x) \tag{3.47}$$

leading to the form (3.9) for $\langle l \rangle$. For α not equal to zero, one has the approximate form

$$\langle l \rangle = \frac{1}{\sqrt{\epsilon}} f(\alpha) . \tag{3.48}$$

Equation (3.48) expresses a scaling property of the problem. If we plot $\sqrt{\epsilon}\langle l \rangle$ versus $g^2/\epsilon^{3/2} = \alpha$ for different values of ϵ, the points should fall on a universal curve. An example of this, for the full logistic map, was shown in Fig. 11. In reality, Eq. (3.48) is not entirely correct since there are corrections to scaling in the problem. More precisely,

$$\langle l \rangle_\alpha = \frac{1}{\sqrt{\epsilon}} F(\alpha, \epsilon) , \tag{3.49}$$

$$f(\alpha) = \lim_{\epsilon \to 0} F(\alpha, \epsilon) . \tag{3.50}$$

The limit in Eq. (3.50) is well-behaved. For small α, $f(\alpha) \sim$ const. For large α, we expect $\langle l \rangle$ to be independent of ϵ; this is only possible if

$$f(\alpha) \sim \frac{1}{\alpha^{1/3}} \quad \text{for } \alpha \to \infty , \tag{3.51}$$

giving

$$\langle l \rangle \sim \frac{1}{g^{2/3}} . \tag{3.52}$$

Note that this is different from what one naively would expect for a random walk

$$y_0 \sim l^{1/2} g \Rightarrow l \sim \frac{y_0}{g^2} . \tag{3.53}$$

The difference is due to the drift term in (3.1), and can be understood as follows: for large y, the drift term dominates while for small y one can assume a pure random walk. To be more precise, the drift term is more important than the noise when $|y| \gtrsim y_c$, while the noise term is more important for $|y| \lesssim y_c$. The crossover value y_c is easily found to be of order $g^{2/3}/a^{1/3}$. The time it takes to go from $-y_0$ to y_c due to drift only is

$$l_1 \sim 1/y_c \sim a^{1/3}/g^{2/3} , \tag{3.54}$$

while the time it takes to go from $-y_c$ to y_c by a pure random walk is

$$l_2 \sim \frac{y_c}{g^2} \sim \frac{1}{a^{1/3} g^{2/3}} . \tag{3.55}$$

Both contributions are of the same order and give the behavior (3.52). Clearly, this will be valid in the regime

$$\epsilon^{3/2} \ll g^2 \ll y_0^3 a . \tag{3.56}$$

For still larger values of g, there is a crossover to a pure random-walk regime satisfying (3.53). We will not consider that regime in what follows.

The solution of Eq. (3.44) yields

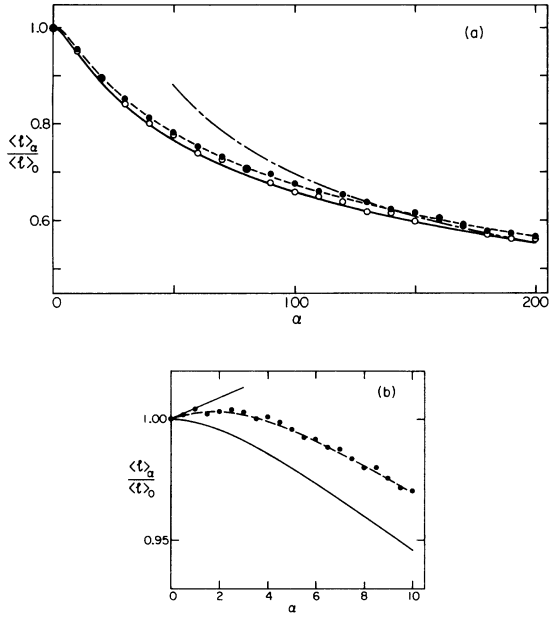

FIG. 17. Average length of passage $\langle l\rangle_\alpha$ normalized to zero noise value $\langle l\rangle_0$ as a function of $\alpha = g^2/\epsilon^{3/2}$, for $z = 2$. The full line is the scaling limit result Eq. (3.60). (a) The dashed line is the theoretical result for $\epsilon = 10^{-5}$, the dots and open circles are results of numerical experiments for $\epsilon = 10^{-5}$ and 10^{-6}, respectively (10 000 passes), rms deviation $\lesssim 0.01$. The dash-dotted line is the asymptotic behavior $\alpha^{-1/3}$. (b) Detailed behavior for small α. Dashed line: theory, $\epsilon = 5\times 10^{-5}$. Dots: numerical simulation, 200 000 passes, rms deviation $\lesssim 0.002$. Straight line: slope at $\alpha = 0$, from Eq. (3.61).

$$m(x) = \frac{2}{\alpha}\int_x^{x_2} d\bar{x}\int_{x_1}^{\bar{x}} dx' e^{-(2/\alpha)[\bar{x}-x'+(\alpha/3)(\bar{x}^3-x'^3)]} - f_0\int_x^{x_2} d\bar{x}\, e^{-(2/\alpha)[\bar{x}+(\alpha/3)x^{-3}]}. \quad (3.57)$$

f_0 is determined by the condition $m(x_1) = 0$; from (3.57), one finds that f_0 is exponentially small so that we will neglect it in what follows. The scaling function is given by

$$f(\alpha) = \frac{1}{2y_0}\lim_{\epsilon\to 0}\sqrt{\epsilon}\int_{-y_0/\sqrt{\epsilon}}^{y_0/\sqrt{\epsilon}} dx\, m(x) = \tfrac{1}{2}m(-\infty) \quad (3.58)$$

or

$$f(\alpha) = \frac{1}{\alpha}\int_x^{\infty} d\bar{x}\int_{-\infty}^{x} dx' e^{-(2/\alpha)[x-x'+(\alpha/3)(x^3-x'^3)]}. \quad (3.59)$$

One can evaluate one of the integrals in (3.59) analytically by changing variables to get

$$f(\alpha) = \left(\frac{\pi}{2\alpha}\right)^{1/2}\int_0^{\infty}\frac{du}{u^{1/2}} e^{-2[u+(\alpha\alpha^2/12)u^3]}. \quad (3.60)$$

This is plotted in Fig. 17 as a full line and the dash-dot curve shows the large α behavior $1/\alpha^{1/3}$. We show also in Fig. 17 the results of numerical experiments for $\epsilon = 10^{-5}$ and $\epsilon = 10^{-6}$. The statistical error in those data (obtained from averaging over 10 000 passages) was $\lesssim 0.01$. As we can see, scaling is approximately satisfied. The dashed line is the theoretical result obtained using the full solution Eq. (3.57) for a finite ϵ, $\epsilon = 10^{-5}$. The corresponding numerical results fit this curve extremely well. It can be seen that small deviations from the scaling limit Eq. (3.60) are evident even for this small value of ϵ.

It is interesting to expand the result (3.57) to lowest order around $\alpha = 0$. One finds

$$\frac{F(\alpha,\epsilon)}{F(0,\epsilon)} = 1 + \frac{1}{8}\frac{\sqrt{\epsilon}\alpha}{y_0} + O(\alpha^2) + O(\epsilon). \quad (3.61)$$

Thus, we see that corrections to scaling in fact give an *increase* in $F(\alpha,\epsilon)$ with respect to its $\alpha = 0$ value for small α. This implies that a small amount of noise actually *increases* the average time of passage, contrary to what one might have expected. This effect is shown in Fig. 17(b) for $\epsilon = 5\times 10^{-5}$. The straight line is the slope at $\alpha = 0$ given by (3.61), the dashed line is obtained from the integral (3.57), and the points are a numerical experiment with 200 000 passes each. The statistical error here is $\lesssim 0.002$. Again, the agreement between theory and experiment is excellent, and one can clearly notice the initial rise of the curve for small α. On this scale of resolution, the difference between the finite ϵ results and the limiting scaling function [given by the full line in Fig. 17(b)] is substantial. Note that in the $\epsilon = 0$ limit, the scaling function $f(\alpha)$ is a monotonically *decreasing* function of α.

We have also computed numerically the probability distribution of path lengths in the presence of external noise. An example is shown as the dash-dotted line in Fig. 15. Note that for the value of $\alpha = 100$ used in this calculation, the average path length is shorter than in the absence of noise. Nevertheless, the probability distribution has a long tail, and it is now possible to observe arbitrarily long path lengths. Note also that in the presence of noise the average path length is close to a peak in the distribution, so that experimentally one will observe predominantly either very short passes or lengths close to the average path length. Thus, although the increase in $P(l)$ for small l is not removed by the presence of noise, the increase for l near $l_{\max}(\alpha = 0)$ disappears.

Finally, we discuss briefly the extension of these results to arbitrary values of z in Eq. (3.1). It is easy to show that the appropriate variable in this case is

$$\alpha = g^2/\epsilon^{(1+1/z)} \tag{3.62}$$

and the scaling form for the average time of passage is

$$\langle l\rangle = \frac{1}{\epsilon^{(1-1/z)}} f(\alpha) \tag{3.63}$$

with

$$f(\alpha) \underset{\alpha\to 0}{\longrightarrow} \text{const}, \tag{3.64a}$$

$$f(\alpha) \underset{\alpha\to\infty}{\longrightarrow} \frac{1}{\alpha^{(z-1)/(z+1)}} . \tag{3.64b}$$

Thus, the behavior for small and large values of the noise is

$$\langle l\rangle \sim \frac{1}{\epsilon^{(1-1/z)}}, \quad \alpha \ll 1 \tag{3.65a}$$

$$\langle l\rangle \sim \frac{1}{g^{2(z-1)/(z+1)}}, \quad \alpha \gg 1 . \tag{3.65b}$$

Note that (3.65b) approaches the free random walk result as $z = \infty$. The solution of the differential equation for general z is

$$m(x) = \frac{2}{\alpha}\int_x^{x_2} dy \int_{x_1}^{x} dy' \exp\!\left(-(2/\alpha)\{y - y' + [a/(z+1)](y^{z+1} - y'^{z+1})\}\right), \quad x_2 = -x_1 = y_0/\epsilon^{1/z} \tag{3.66}$$

and the average time of passage is

$$\langle l\rangle = \frac{1}{2y_0}\frac{1}{\epsilon^{1-2/z}}\int_{x_1}^{x_2} dx\, m(x) . \tag{3.67}$$

In Fig. 18 we show an example of results for $z = 4$. Here, times of passage are much longer so that it is more difficult to get good statistics. The statistical error in the numerical results is ~0.03, with runs of 1000 passes each. As before, the dashed-dot curve in Fig. 16 shows the asymptotic behavior of the scaling function, in this case $1/\alpha^{3/5}$. Again we obtain excellent agreement with the theoretical prediction Eq. (3.67).

IV. CONCLUSION

The approach to aperiodic or chaotic behavior via intermittency which has been discussed here provides a simple model clearly exhibiting the essential characteristics which have made the analysis of one-dimensional maps interesting. First there are a set of clearly defined features for the purely deterministic map which signal the onset of chaos. The average length, as well as the maximum length, of steps associated with a fixed acceptance gate vary as $(R_c - R)^{(1/z-1)}$ as $R_c - R \to 0$. Here z is the parameter characterizing the universality class of the map. Furthermore, in the presence of noise, we have shown that this average length of the laminar regions scales so that

$$\lim_{\epsilon\to 0} \epsilon^{(1-1/z)}\langle l\rangle_\alpha = f(\alpha) \tag{4.1}$$

with $\alpha = g^2/\epsilon^{(1+1/z)}$, $f(0) = \text{const}$, and $f(\alpha) \sim \alpha^{-(z-1)/(z+1)}$ for $\alpha \gg 1$. Here, as opposed to the bifurcation cascade the "critical indices" are rational numbers. One should not however think of this as a mean-field behavior. In fact for the case of the logistic map where $z = 2$, the scaling relations are analogous to those of Pott's model near its multicritical point.[20]

We have also studied how corrections to scaling enter and in particular how they give rise to an initial increase in $\langle l\rangle_\alpha$ for small α. It is important to have an idea of the size of these effects since any real system is bound to have some external noise acting on it.

Besides the characteristic length and the correlation function and its power spectrum, we have studied the behavior of the distribution of lengths $P(l)$ and the stationary probability distribution $W(x)$. In the absence of external noise, the deep valley in $P(l)$ near $\langle l\rangle$ provides a possible flag for

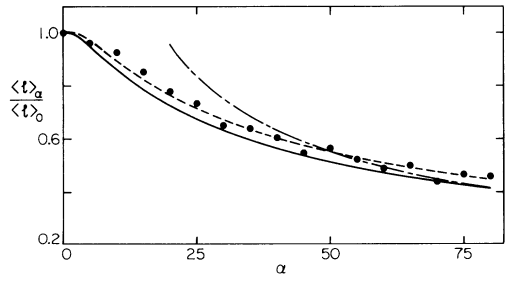

FIG. 18. For $z = 4$ the average length of passage $\langle l\rangle_\alpha$ normalized to the zero noise value $\langle l\rangle_0$ is plotted as a function of $\alpha = g^2/\epsilon^{5/4}$. Here $y_0 = 0.1$. Dashed line: theory, $\epsilon = 10^{-5}$. Dots: numerical simulation, $\epsilon = 10^{-5}$, 1000 passes, rms deviation $\lesssim 0.03$. Full line: scaling limit. Dash-dotted line: asymptotic behavior $\alpha^{-3/5}$.

this type of intermittency. However, in the presence of external noise, it is clear from Figs. 7 and 15 that real care must be exercised in using $P(l)$ to prove that observed intermittency[21] is or is not of the type discussed here.

Finally, just as in the case of phase transitions, we have seen that one must be careful to be inside the critical region in order to compare data with the various leading exponents and scaling relations derived here. In the case of $\langle l \rangle_0$, this critical region was set by requiring that $\sqrt{\epsilon/a}$ be sufficiently small compared to the gate y_0 that $(\pi/2)\arctan(y_0/\sqrt{\epsilon/a}) \cong 1$. However the Lyapunov exponent exhibited a substantially narrower critical region for $\epsilon > 0$.

Clearly, in spite of the numerical tests reported here which provide strong confirmation for the analytic results, the real test of these ideas will be experimental. To the authors present knowledge, the intermittent behavior so far reported does not in fact fit the type of results described here.[22] Hopefully, physical systems falling within this universality class will be found so that these ideas can be tested further.

ACKNOWLEDGMENTS

One of the authors (D.J.S.) would particularly like to thank M. Nauenberg for point out to him the similarity between the ideas of Y. Pomeau and P. Manneville and the behavior of the two-dimensional Potts model near its multicritical point which stimulated his interest in this problem. We would also like to acknowledge helpful discussions with H. Abarbanel, G. Ahlers, M. Feigenbaum, L. Kadanoff, and A. Libchaber. We are also grateful to J.-P. Eckman, L. Thomas, and P. Wittwer for sending us a copy of their paper prior to publication. J. Hirsch would like to acknowledge support from the NSF under Grant No. PHY77-27084, and D. J. Scalapino would like to acknowledge the support of the ONR under Contract No. N00014-79-C-0707. One of us (D.J.S.) would also like to thank Xerox PARC for their generous hospitality and the use of their computing facilities where the numerical work on the logistic map was carried out. He would also like to thank A. Zisook for his help.

[1]R. May, Nature (London) 261, 459 (1976).
[2]M. Feigenbaum, J. Stat. Phys. 19, 25 (1978); 21, 669 (1979).
[3]P. Collet and J. P. Eckmann, *Iterated Maps on the Interval as Dynamical Systems* (Birkhäuser, Basel, 1980).
[4]E. N. Lorenz, J. Atmos. Sci. 20, 130 (1963).
[5]P. Bak, Phys. Rev. Lett. 46, 791 (1981).
[6]E. Fradkin and B. A. Huberman (unpublished).
[7]S. Aubry, *Annals of the Israel Physical Society*, edited by C. G. Kuper (Adam Hilger, Bristol, 1979), Vol. 3, p. 133.
[8]M. Feigenbaum, Los Alamos Sci. Mag. 1, 4 (1980).
[9]B. A. Huberman and J. Rudnick, Phys. Rev. Lett. 45, 154 (1980).
[10]P. Manneville and Y, Pomeau, Phys. Lett. 75A, 1 (1979); Commun. Math. Phys. 74, 189 (1980).
[11]G. Mayer-Kress and H. Haken (unpublished).
[12]T. Li and J. A. Yorke, Am. Math. Monthly 82, 985 (1972).
[13]J. P. Crutchfield and B. A. Huberman, Phys. Lett. 77A, 407 (1980).
[14]J. P. Crutchfield, M. Nauenberg, and J. Rudnick, Phys. Rev. Lett. 46, 933 (1981).
[15]B. Shraiman, C. E. Wayne, and P. C. Martin, Phys. Rev. Lett. 46, 935 (1981).
[16]B. A. Huberman and A. Zisook, Phys. Rev. Lett. 46, 626 (1981); J. P. Crutchfield, J. D. Farmer, and B. A. Huberman (unpublished).
[17]After this work was completed we received some unpublished work from J. P. Eckmann, L. Thomas, and P. Wittwer in which some of the results reported here were also obtained.
[18]R. Graham, in *Quantum Statistics in Optics and Solid-State Physics*, Vol. 66 of *Springer Tracts in Modern Physics* (Springer, Berlin, 1973), Vol. I.
[19]R. L. Stratonovich, *Topics in the Theory of Random Noise* (Gordon and Breach, New York, 1963), Vol. I.
[20]J. Cardy, M. Nauenberg, and D. J. Scalapino, Phys. Rev. B 22, 2560 (1980).
[21]Intermittency in certain parameter regions of the Raleigh-Benard experiments of A. Libchaber and J. Mauer evidently does not exhibit the characteristics of the model discussed here (A. Libchaber, private communication).
[22]G. Ahlers (unpublished).